



This is a repository copy of *Modelling the effect of submarine iceberg melting on glacier-adjacent water properties*.

White Rose Research Online URL for this paper:
<https://eprints.whiterose.ac.uk/184113/>

Version: Submitted Version

Article:

Davison, B.J. orcid.org/0000-0001-9483-2956, Cowton, T. orcid.org/0000-0003-1668-7372, Sole, A. orcid.org/0000-0001-5290-8967 et al. (2 more authors) (Submitted: 2021)
Modelling the effect of submarine iceberg melting on glacier-adjacent water properties.
The Cryosphere Discussions. (Submitted)

<https://doi.org/10.5194/tc-2021-323>

Reuse

This article is distributed under the terms of the Creative Commons Attribution (CC BY) licence. This licence allows you to distribute, remix, tweak, and build upon the work, even commercially, as long as you credit the authors for the original work. More information and the full terms of the licence here:
<https://creativecommons.org/licenses/>

Takedown

If you consider content in White Rose Research Online to be in breach of UK law, please notify us by emailing eprints@whiterose.ac.uk including the URL of the record and the reason for the withdrawal request.



eprints@whiterose.ac.uk
<https://eprints.whiterose.ac.uk/>



1 **Modelling the effect of submarine iceberg melting on glacier-adjacent**
2 **water properties**

3 **Benjamin Davison^{1,2}, Tom Cowton¹, Andrew Sole³, Finlo Cottier^{4,5}, Pete Nienow⁶**

4 ¹Department of Geography and Sustainable Development, University of St Andrews, St Andrews, UK

5 ²School of Earth and Environment, University of Leeds, Leeds, UK

6 ³Department of Geography, University of Sheffield, Sheffield, UK

7 ⁴Scottish Association for Marine Science, Scottish Marine Institute, Oban, UK

8 ⁵Department of Arctic and Marine Biology, UiT The Arctic University of Norway, Tromsø, Norway

9 ⁶School of Geosciences, University of Edinburgh, Edinburgh, UK

10 Correspondence email: b.davison@leeds.ac.uk

11

12 **Abstract**

13 The rate of ocean-driven retreat of Greenland's tidewater glaciers remains highly uncertain in
14 predictions of future sea level rise, in part due to poorly constrained glacier-adjacent water properties.
15 Icebergs and their meltwater contributions are likely important modifiers of fjord water properties, yet
16 their effect is poorly understood. Here, we use a 3-D ocean circulation model, coupled to a submarine
17 iceberg melt module, to investigate the effect of submarine iceberg melting on glacier-adjacent water
18 properties in a range of idealised settings. Submarine iceberg melting can modify glacier-adjacent water
19 properties in three principle ways: (1) substantial cooling and modest freshening in the upper ~50 m of
20 the water column; (2) warming of Polar Water at intermediate depths due to iceberg melt-induced
21 upwelling of warm Atlantic Water, and; (3) warming of the deeper Atlantic Water layer when vertical
22 temperature gradients through this layer are steep (due to vertical mixing of warm water at depth), but
23 cooling of the Atlantic Water layer when vertical temperature gradients are shallow. The overall effect
24 of iceberg melt is to make glacier-adjacent water properties more uniform with depth. When icebergs
25 extend to, or below, the depth of a sill at the fjord mouth, they can cause cooling throughout the entire
26 water column. All of these effects are more pronounced in fjords with higher iceberg concentrations
27 and deeper iceberg keel depths. These iceberg melt-induced changes to glacier-adjacent water
28 properties will reduce rates of glacier submarine melting near the surface, but increase them in the Polar
29 Water layer, and cause typically modest impacts in the Atlantic Water layer. These results characterise
30 the important role of submarine iceberg melting in modifying ice sheet-ocean interaction, and highlight
31 the need to improve representations of fjord processes in ice sheet-scale models.

32



33 **1. Introduction**

34 Predicting the rates of ocean-driven retreat of Greenland's tidewater glaciers remains one of the largest
35 uncertainties in estimating future sea level rise (Edwards et al., 2021; Meredith et al., 2020). This
36 uncertainty is partly due to limited constraints on the ocean-driven thermal forcing of tidewater glacier
37 calving fronts, which reflects in part the difficulty in obtaining hydrographic observations in the
38 proximity of tidewater glacier termini (Jackson et al., 2017, 2020; Sutherland et al., 2019). The few
39 observations of water properties in the inner part of glacial fjords demonstrate that there are typically
40 substantial differences between glacier-adjacent water properties and those near the fjord mouth (e.g.
41 Inall et al., 2014; Jakobsson et al., 2020; Straneo et al., 2011), indicating that substantial modification
42 of water temperature and salinity can occur within glacial fjords. Due to the relatively small number of
43 observations and insufficient model constraints on glacier-adjacent water properties, ice sheet models
44 used to simulate glacier retreat must be forced with far-field (i.e. acquired on and beyond the continental
45 shelf) ocean boundary conditions that do not include fjord-scale influences (Goelzer et al., 2020; Slater
46 et al., 2019), thereby introducing uncertainty into the resulting projections of ice sheet mass loss.

47 Glacier-adjacent water properties can differ from those near the fjord mouth for several reasons.
48 Meltwater runoff enters the fjord at depth where tidewater glaciers meet the ocean ('subglacial
49 discharge'). In Greenland's fjords, warm water of Atlantic origin (Atlantic Water, AW) is generally
50 found at depth, whilst colder, fresher water of Polar origin (Polar Water, PW) is found at intermediate
51 depths (Straneo and Heimbach, 2013; Sutherland and Pickart, 2008). The cold, fresh subglacial
52 discharge is buoyant when it enters the fjord, so rises as a turbulent plume (Jenkins, 2011). As it rises,
53 it entrains fjord water, which mixes with the subglacial discharge as it ascends towards the fjord surface
54 (e.g. Beaird et al., 2018). In this way, subglacial discharge-driven plumes act as mixing engines at the
55 head of glacial fjords. Due to the temperature stratification in Greenland's fjords, plumes at deeply-
56 grounded glaciers (i.e. deeper than the PW-AW interface) often draw the relatively warm AW towards
57 the fjord surface, thereby warming surface and near-surface waters (e.g. Carroll et al., 2016; Straneo et
58 al., 2010, 2011). In contrast, plumes at shallowly-grounded glaciers can cause cooling at and near the
59 fjord surface, as cold subglacial discharge and entrained PW is upwelled into surface layers that are
60 seasonally warmed by solar radiation (Carroll et al., 2016). Models that include glacial plumes are able
61 to reproduce these effects convincingly (Carroll et al., 2016; Cowton et al., 2015; Jackson et al., 2017).
62 However, there remain substantial differences between modelled water properties and those that are
63 observed adjacent to tidewater glaciers (Cowton et al., 2016; Davison et al., 2020; Fraser and Inall,
64 2018).

65 Several recent studies have identified icebergs as a substantial freshwater source in some of Greenland's
66 fjords, with iceberg freshwater volumes comparable to or greater than ice sheet runoff (Enderlin et al.,
67 2016, 2018; Jackson and Straneo, 2016; Moon et al., 2017; Moyer et al., 2019; Rezvanbehbahani et al.,
68 2020). Furthermore, modelling of one of these fjords suggests that including the heat and salt fluxes



69 associated with submarine iceberg melting increases greatly the model's ability to reproduce observed
70 glacier-adjacent water properties (Davison et al., 2020). However, iceberg concentration, keel depth,
71 and size-frequency distribution likely vary hugely between fjords as well as over time, though
72 observations of icebergs at the fjord scale are sparse (Enderlin et al., 2016; Moyer et al., 2019;
73 Rezvanbehbahani et al., 2020; Sulak et al., 2017). As such, it is likely that the effect of icebergs on
74 glacier-adjacent water properties will also vary both spatially (i.e. between fjords) and temporally. This
75 variability likely results in different thermal forcing of tidewater glaciers for a given set of far-field
76 ocean conditions. Constraining the effect of icebergs on glacier-adjacent water properties, and thus
77 glacier submarine melt rates, is therefore a necessary step in order to improve projections of ice sheet
78 mass loss.

79 Here, we use an ocean circulation model in a series of idealised fjord-scale simulations to examine how
80 icebergs affect glacier-adjacent water properties across a range of Greenland-relevant scenarios. We
81 first consider how iceberg concentration, keel depth and size-frequency distribution individually affect
82 glacier-adjacent water properties. We then consider a range of representative iceberg and ocean
83 scenarios, to examine how these parameters interact to determine water properties in the critical region
84 adjacent to tidewater glacier termini. Greenland's fjords are complex and varied in their geometry,
85 ranging from short, narrow inlets to those that are long and wide, each with varying sinuosity and
86 bathymetry, and often with several tributaries and sills of varying depth along their length. It would be
87 impractical to attempt to characterise all of these systems. Therefore, we focus here on two simple fjord
88 geometries: one with no sills and another with a single entrance sill, which we expect to be of particular
89 importance for iceberg-ocean interaction given the capacity of sills to concentrate fjord-shelf water
90 exchange near the surface where icebergs are concentrated.

91

92 **2. Methods**

93 **2.1. Model domain**

94 We use the Massachusetts Institute of Technology general circulation model (MITgcm) in its non-
95 hydrostatic configuration (Marshall et al., 1997a, 1997b) to model submarine ice melting and circulation
96 in an idealised fjord 50 km in length and 5 km in width. In most simulations, the domain is uniformly
97 500 m deep. However, in some simulations, we include a sill which limits the overlying water depth to
98 100 m (uniform across the entire width of the fjord, and approximately 5 km wide in the along-fjord
99 direction, with a Gaussian profile), centred 10 km from the open boundary (Fig. 1a). Model resolution
100 is uniformly 500 m horizontally and 10 m vertically. The fjord sides are closed boundaries, while at the
101 open ocean boundary we impose a 5 km sponge layer, in which conditions are relaxed towards those
102 imposed at the boundary (e.g. Cowton et al., 2016; Sciascia et al., 2013; Slater et al., 2015). The glacier-
103 end of the domain is closed and consists of a virtual ice wall 5 km wide and 500 m high. In simulations

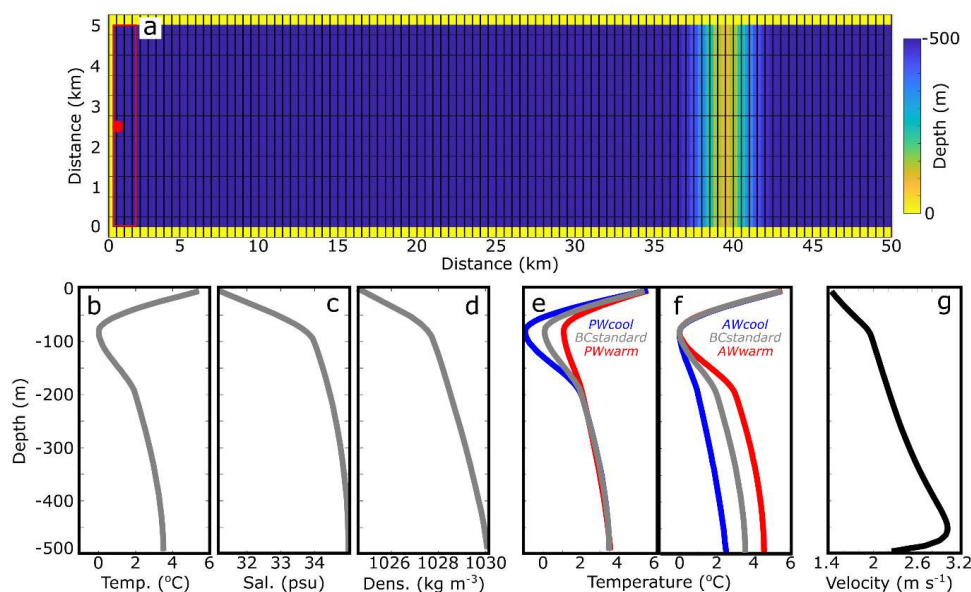


Figure 1. Model domain and boundary conditions. (a) Plan-view of model bathymetry with sill, with the ice wall at the left end of the domain (0 km) and the open boundary on the right. Hatching indicates model resolution (note that grid cells are 500 m x 500 m in the horizontal). The red dot marks the location of subglacial discharge injection and the red box indicates the region from which steady-state glacier-adjacent water properties were extracted. In simulations without a sill, the domain is uniformly 500 m deep. Vertical profiles of (b) temperature, (c) salinity and (d) density with *BCstandard*. (e) Temperature profiles with varying PW temperature. (f) Temperature profiles with varying AW temperature. (g) Example plume vertical velocity from the simulation with iceberg scenario five, 500 m³ s⁻¹ runoff and *BCstandard* boundary conditions.

104 incorporating runoff, this is input at a rate of 500 m³ s⁻¹, a value typical of many of Greenland's tidewater
105 glaciers (Mankoff et al., 2020), at the centre of the base of the ice wall (Fig. 1a). The velocity of the
106 runoff-driven plume (e.g. Fig. 1g) and the melting of the ice wall were calculated using the 'IcePlume'
107 package (Cowton et al., 2015). In common with several previous studies (Kimura et al., 2014; Slater et
108 al., 2015; Xu et al., 2013), we implement a free slip condition on the fjord walls and ice front and do
109 not simulate the effects of sea ice, atmospheric forcing or tides.

110 2.2. Initial and open boundary conditions

111 We use idealised representations of temperature and salinity profiles commonly observed at the mouth
112 of Greenland's south-eastern fjords during late-summer as initial and open boundary conditions
113 (Sutherland et al., 2014). In our standard setup, this idealised profile is a cubic interpolation between
114 6°C and 31 psu at the fjord surface, 0°C and 34 psu at 100 m depth, 2°C at 200 m and 3.5°C at 500 m
115 depth, where salinity is greatest at 35 psu (Fig. 1b-d). In this way, the upper several tens of metres
116 represent waters that are seasonally warmed by solar insolation, whilst the relatively cold intermediate

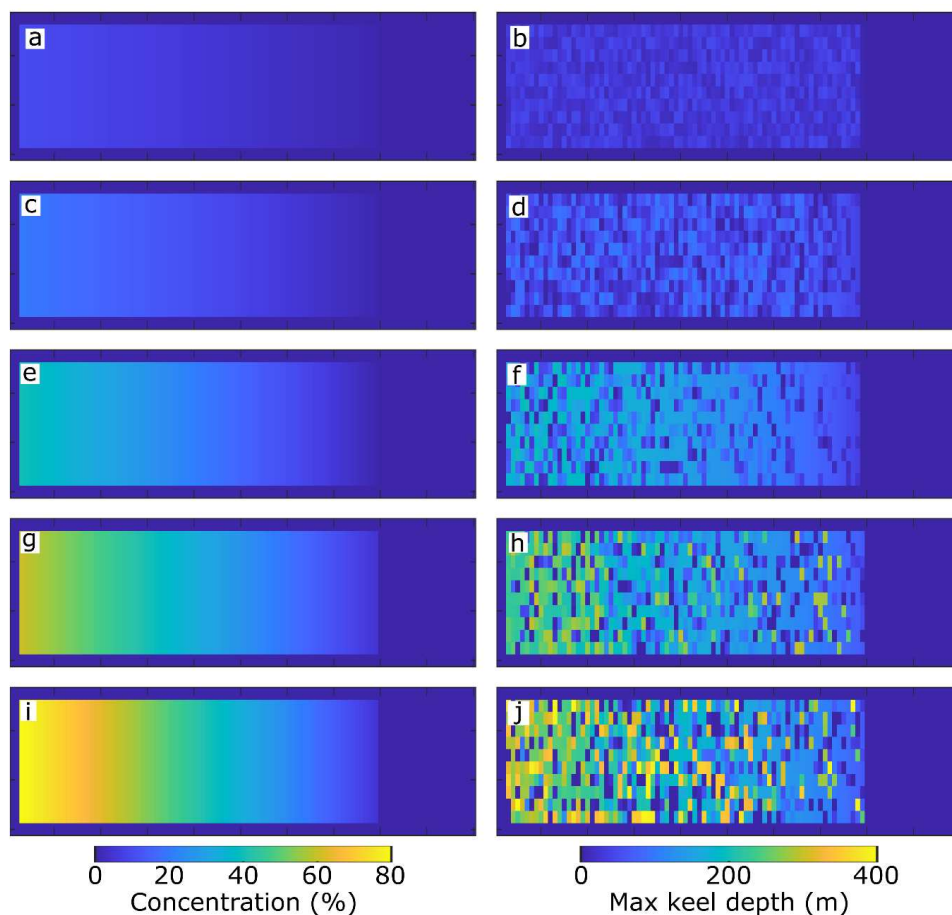


Figure 2. Iceberg concentration (left column) and maximum iceberg keel depth (right column) for iceberg scenarios one to five (top to bottom). All panels show the domain in plan-view, and are 50 km long and 5 km across.

117 layer, centred 100 m below the fjord surface, represents the PW layer, which is underlain by warmer,
118 more saline water representing the AW layer. Henceforth, we refer to this set of boundary conditions
119 as *BCstandard*. In separate simulations, we use temperature minima at 100 m of -1°C (*PWcool*) and
120 1°C (*PWwarm*) and temperature maxima at 500 m of 2.5°C (*AWcool*) and 4.5°C (*AWwarm*) (Fig. 1e,f).
121 Changing the temperature of the AW and PW layers causes corresponding changes in the vertical
122 temperature gradient (Fig. 1e,f), the effects of which are discussed in Sect. 3.2. Initial and open
123 boundary salinity is kept constant between simulations, but density changes between simulations are
124 negligible. Boundary conditions were kept constant throughout each simulation.

125



Table 1. Details of each iceberg scenario. Concentration is the percentage of the fjord in plan-view occupied by icebergs. Iceberg concentration was linearly interpolated from the maximum value (adjacent to the glacier wall) to the minimum value 40 km down fjord.

Iceberg scenario	Max. draught (m)	Exponent	Concentration [max,min] (%)	Surface area (km ²)
Scenario 1	50	1.6	[10,1]	44.5
Scenario 2	100	1.7	[20,1]	76.5
Scenario 3	200	1.8	[40,1]	141
Scenario 4	300	1.9	[60,5]	235
Scenario 5	400	2.1	[80,5]	316

126 2.3. Iceberg-ocean interaction

127 Submarine iceberg melting is simulated using the ‘IceBerg’ package within MITgcm (Davison et al.,
128 2020), with an ice temperature of -10°C (Inall et al., 2014; Luthi et al., 2002; Sciascia et al., 2013;
129 Sutherland and Straneo, 2012). This package uses the velocity-dependent three-equation melt rate
130 parameterisation (Holland and Jenkins, 1999; Xu et al., 2012) to resolve the vertical pattern of
131 submarine melting of individual icebergs. The temperature and salinity fluxes associated with melting
132 of individual iceberg faces within a grid cell are calculated based on local temperature, salinity and
133 face-normal velocity. Face-normal current speed is calculated assuming that icebergs drift with the
134 average current velocity along their draught (though we note that the iceberg locations are kept constant
135 through each simulation). Melt-driven plumes are not simulated directly; instead, their effect on melt
136 rates is parameterised by applying a minimum face-normal current speed of 0.06 m s^{-1} to each iceberg
137 face. This minimum current speed is based on line plume modelling (Davison et al., 2020). The package
138 does not include the effect of waves or mechanical iceberg breakup; therefore, melt rates calculated
139 here are conservative. We use standard parameter values (Cowton et al., 2015; Davison et al., 2020;
140 Jackson et al., 2020) for the drag coefficient (0.0025), and thermal and salt turbulent transfer coefficients
141 (0.022 and 0.00062, respectively). The icebergs are rectangular in plan-view and have flat, vertical
142 sides. All icebergs have length, l , to width ratios of 1.62:1 (Dowdeswell et al., 1992), and iceberg keel
143 depth, d , is related to iceberg length through, $d=2.91l^{0.71}$ (Barker et al., 2004).

144 In Sect. 3.1, we consider a range of iceberg concentrations, maximum keel depths and size-frequency
145 distributions, whilst using only the *BCstandard* boundary conditions. In all setups, iceberg
146 concentration is uniform across the fjord and decreases linearly from a maximum adjacent to the virtual
147 ice wall to a minimum 10 km from the open boundary. In Sect. 3.1, iceberg concentration (defined as
148 the percentage of the fjord surface in plan-view occupied by icebergs), is 80% adjacent to the ice wall
149 and decreases to 5% in our *c1* experiment, and is reduced to 75, 50 and 25% of these values in our
150 *c0.75*, *c0.5*, and *c0.25* experiments, respectively. Regardless of concentration, we use a maximum
151 iceberg keel depth of 300 m and the size-frequency distribution of the icebergs is described using a



152 power law with an exponent of -2, which is similar to that observed in Sermilik Fjord (Sulak et al.,
153 2017). In separate simulations, we assign maximum iceberg keel depths of 50 m, 150 m, 250 m, 350 m
154 and 450 m, whilst maintaining the cI concentration and the -2 power law exponent. We then vary the
155 size-frequency distribution power law exponent from -1.6 to -2.1 in increments of 0.1 (covering the
156 range observed to date in Greenland's fjords (Rezvanbehbahani et al., 2020; Sulak et al., 2017)), whilst
157 retaining the cI concentration and the 300 m maximum keel depth.

158 In Sect. 3.2 onwards, we consider five realistic combinations of iceberg concentration, maximum
159 iceberg keel depth and power law exponent, in order to approximate the range of iceberg geometries
160 and distributions found in Greenland's fjords (Fig. 2). These iceberg setups range from those
161 representing a fjord hosting few and small icebergs, such as Kangerlussuup Sermia Fjord (Sulak et al.,
162 2017) (scenario one), to those representing an iceberg-congested fjord, such as Sermilik Fjord (scenario
163 five) (Fig. 2; Table 1).

164

165 3. Results

166 3.1. The effect of iceberg concentration, keel depth and size-frequency distribution on glacier- 167 adjacent water properties

168 The effect of iceberg melt on glacier-adjacent water properties depends on iceberg geometry, iceberg
169 concentration and iceberg size-frequency distribution (Fig. 3), as well as on the presence or absence of
170 subglacial discharge. In the absence of subglacial discharge, icebergs modify glacier-adjacent water
171 properties (here defined as the average properties of the water within 2 km of the ice wall; Fig. 1a) in
172 two main ways. Firstly, they cause substantial (6-7.5°C) cooling in the upper ~60 m of the water column,
173 relative to the initial conditions (Fig. 3a-c). The amount of cooling in this near-surface layer depends
174 somewhat on iceberg concentration, with steady-state water temperature varying between ~-1.5°C and
175 ~0°C over the range of iceberg concentrations considered, but is otherwise relatively insensitive to
176 changing iceberg geometry and distribution (Fig. 3a-c). Secondly, warming of up to ~1°C occurs below
177 ~80 m because iceberg melting causes localised freshening at depth. The resulting iceberg melt-
178 modified water (i.e. the mixture of iceberg freshwater and ambient water at depth) is less dense than the
179 surrounding water and rises buoyantly towards the fjord surface. The vertical extent and magnitude of
180 the resulting warming generally increase with maximum iceberg keel depth (Fig. 3b), because icebergs
181 with deeper keels cause upwelling of deeper AW (which in this case is also warmer (Fig. 1b)). This
182 warming effect does not extend to the fjord surface, because the stronger stratification near the surface
183 limits upwelling and because iceberg-ocean contact areas are much greater near the surface, so cooling
184 due to localised iceberg melting dominates. When subglacial discharge is included, the effect of iceberg
185 melt on glacier-adjacent water properties at depth (below 60 m) is similar to that in simulations without
186 subglacial discharge, but glacier-adjacent water temperatures in the upper ~60 m of the water column
187 display a greater range and the cooling of the near-surface waters is considerably reduced (Fig. 3d-f).

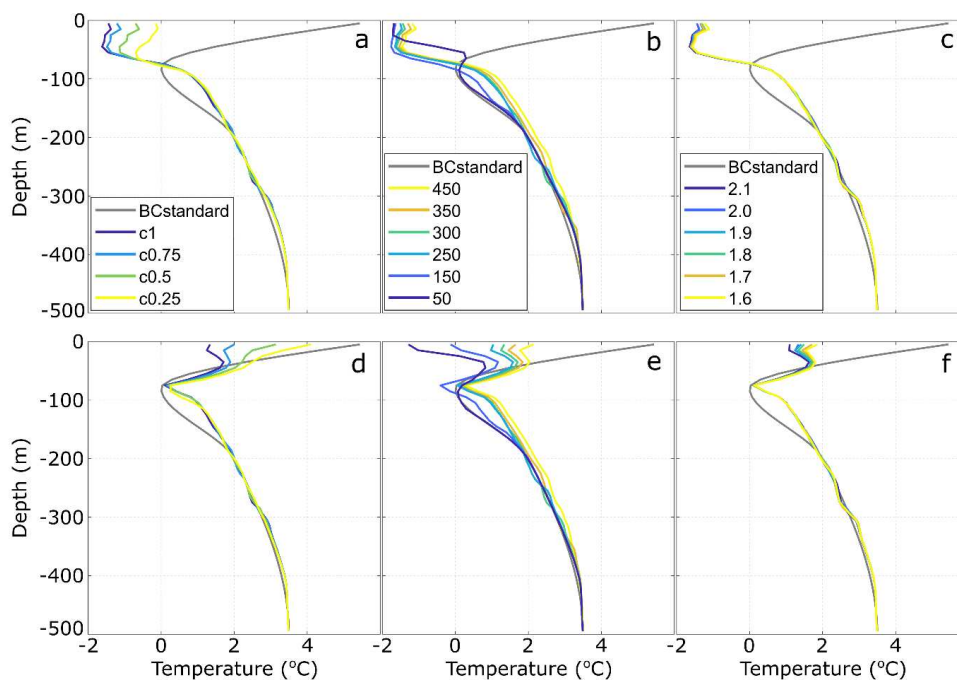


Figure 3. Glacier-adjacent water temperature vs iceberg geometry and distribution. Effect of iceberg concentration (a & d), maximum iceberg draught (b & e) and exponent describing the size-frequency distribution (c & f). Panels (a-c) are for simulations without runoff, whilst panels (d-f) are for simulations with $500 \text{ m}^3 \text{ s}^{-1}$ runoff.

188 This is because the runoff causes strong upwelling of AW towards the fjord surface and increases rates
189 of fjord-shelf exchange, which counters some of the iceberg-induced cooling of near-surface waters.

190

191 3.2. Combining iceberg scenarios and ocean conditions

192 In reality, changes in iceberg concentration, keel depth and size-frequency distribution do not occur in
193 isolation and there are characteristic relationships between those iceberg descriptors (Sulak et al., 2017).
194 Fjords hosting large glaciers, such as Sermilik Fjord and Helheim Glacier in east Greenland, tend to
195 contain both high iceberg concentrations and large, deeply-draughted icebergs, whilst those with lower
196 iceberg concentrations, such as Kangerlussuup Sermia Fjord, also tend to contain smaller icebergs. To
197 better represent the range of iceberg conditions found in Greenland's fjords, we consider five iceberg
198 'scenarios' (Fig. 2; Table 1), ranging from a fjord with low iceberg concentration, shallow iceberg keels
199 and fairly uniform iceberg sizes (iceberg scenario one), to a fjord with high iceberg concentration, deep
200 iceberg keels and a large range of iceberg sizes (iceberg scenario five). For each of these scenarios, we
201 examine steady-state glacier-adjacent water temperature for a range of ocean boundary conditions, and



202 with and without a shallow (100 m) sill. We therefore consider three different PW and AW temperatures
203 in turn (Fig. 1e,f), and examine the resulting glacier-adjacent water properties for each of the five
204 iceberg scenarios. To isolate the effect of iceberg melting from other processes, we compare each of the
205 above simulations to identical simulations without icebergs.

206

207 3.2.1. Changing Polar Water temperature

208 Fig. 4 shows steady-state glacier-adjacent water properties for the range of iceberg scenarios and PW
209 temperatures considered. In all iceberg scenarios, there is substantial ($\sim 2^{\circ}\text{C}$ or more) cooling in the
210 upper ~ 60 m, with greater cooling in scenarios with higher iceberg concentrations. Other than this near-
211 surface cooling, glacier-adjacent water properties are very similar to open ocean conditions in iceberg
212 scenarios one and two (which have the lowest iceberg concentrations; Fig. 2; Table 1). However, in
213 iceberg scenarios three to five, the PW layer is increasingly modified (Figs 4c-e). With *PWcool*,
214 icebergs in these scenarios cause on average a net *warming* of 1.02°C in the 80-200 m depth range,
215 compared to simulations without icebergs. Conversely, with *PWwarm*, the icebergs cause a net cooling
216 of 0.30°C over the same depth range, such that the steady-state temperature profiles for both sets of
217 initial conditions (*PWcool* and *PWwarm*) are similar. With *BCstandard*, the influence of icebergs on
218 glacier-adjacent water properties falls between the two, with the net effect being a slight (0.43°C)
219 warming (Fig. 4c-e). These changes arise due to differing balances between cooling due to iceberg
220 melting, and warming due to buoyancy-induced upwelling of relatively warm AW water. With *PWcool*
221 there is relatively little iceberg melting in the PW layer (because the PW is close to the *in-situ* freezing
222 point), and so warming due to upwelling of AW dominates (driven by iceberg melting at greater depth
223 in the warmer AW layer). In contrast, with *PWwarm*, iceberg melt rates in the PW layer are
224 comparatively high, and the temperature difference between the PW and AW layers is reduced, so
225 localised cooling offsets warming due to turbulent upwelling. In short, under the conditions represented
226 by these simulations, submarine iceberg melting acts to make glacier-adjacent water temperature more
227 uniform with depth (Fig. 4c-e).

228 The addition of a 100 m deep sill near the fjord mouth serves to amplify the cooling effect of icebergs
229 (Fig. 4f-j). Sills typically block external shelf waters below the sill depth from entering the fjord (unless
230 external forcing causes a shallowing of isopycnals seaward of the sill), causing the fjord basin bounded
231 by the sill to be replenished by waters sourced only from above the sill depth (e.g. Jakobsson et al.,
232 2020). When icebergs reach down to the sill depth, all water entering the fjord may thus be subject to
233 melt-driven cooling. The result is that icebergs cause cooling throughout the water column, even below
234 the deepest iceberg keels and below the sill depth (Fig. 4f-j). This cooling is increasingly pronounced
235 as the PW temperature increases and with more concentrated and deeper icebergs (Fig. 4f-j). For
236 example, over the 100 to 500 m depth range with *PWcool*, icebergs cause 0.21°C cooling on average in

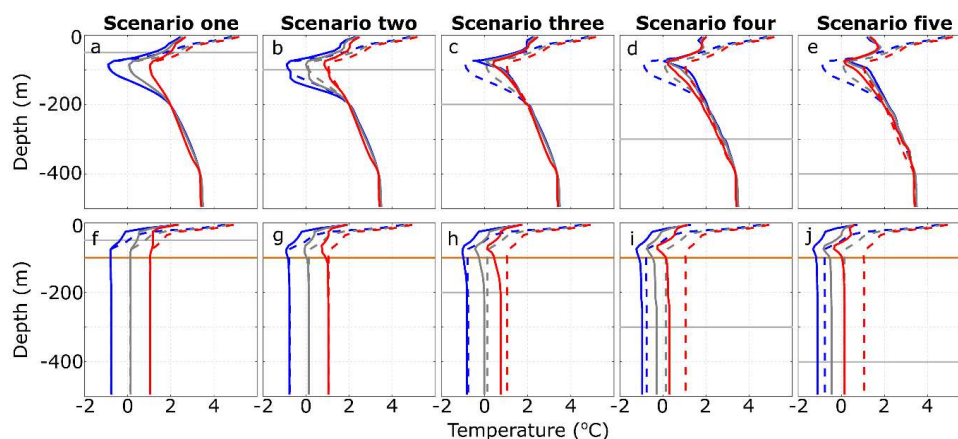


Figure 4. Steady-state glacier-adjacent water temperature for a range of initial Polar Water conditions. In all plots, solid and dashed lines indicate simulations with and without icebergs, respectively. Plots a-e show configurations with a flat-bottomed domain, whilst f-j show those with a 100 m deep sill. Grey, blue and red lines show scenarios using the *BCstandard*, *PWcool* and *PWwarm* boundary conditions respectively (shown in Figure 1e). The horizontal grey lines indicate the maximum iceberg keel depth in each scenario, and the horizontal orange lines in panels f-j indicate the sill depth.

237 iceberg scenarios three to five (0.06°C in scenario three and 0.35°C in scenario five); whilst with
238 *PWwarm*, icebergs cause 0.67°C cooling on average (0.33°C in scenario three and 0.91°C in scenario
239 five).

240 The varied effects of icebergs on glacier-adjacent water properties are apparent in temperature-salinity
241 space (Fig. 5). Initial glacier-adjacent water properties are inherited from those prescribed at the fjord
242 mouth; however, icebergs modify fjord waters through ice melt and meltwater-driven vertical mixing.
243 Comparing temperature-salinity profiles of simulations with and without icebergs illustrates these
244 effects (Fig. 5). In the upper ~ 60 m of all simulations with icebergs, iceberg melting causes substantial
245 cooling and slight freshening (e.g. compare solid and open circles in Fig. 5 – solid circles are drawn
246 down and slightly left in temperature-salinity space). Deeper in the water column (below 100 m), the
247 influence of iceberg melting on water properties depends on the iceberg scenario and the presence or
248 absence of a sill. In iceberg scenario one (Fig. 5a, b), iceberg melting causes very little modification of
249 waters below 100 m, even in the presence of a sill (Fig. 5b). This is because the icebergs do not extend
250 to the sill water depth and so there is some unmodified exchange between the fjord and shelf. In iceberg
251 scenario five, icebergs cause on average 0.19°C warming of waters below 100 m when there is no sill,
252 and cooling of 0.61°C below 100 m when there is a sill (Fig. 5b). This cooling below the maximum
253 iceberg draught occurs in all iceberg scenarios in which icebergs extend to sill depth, but is most
254 apparent in the higher iceberg concentration scenarios (e.g. Fig. 5d). The simulated changes in water

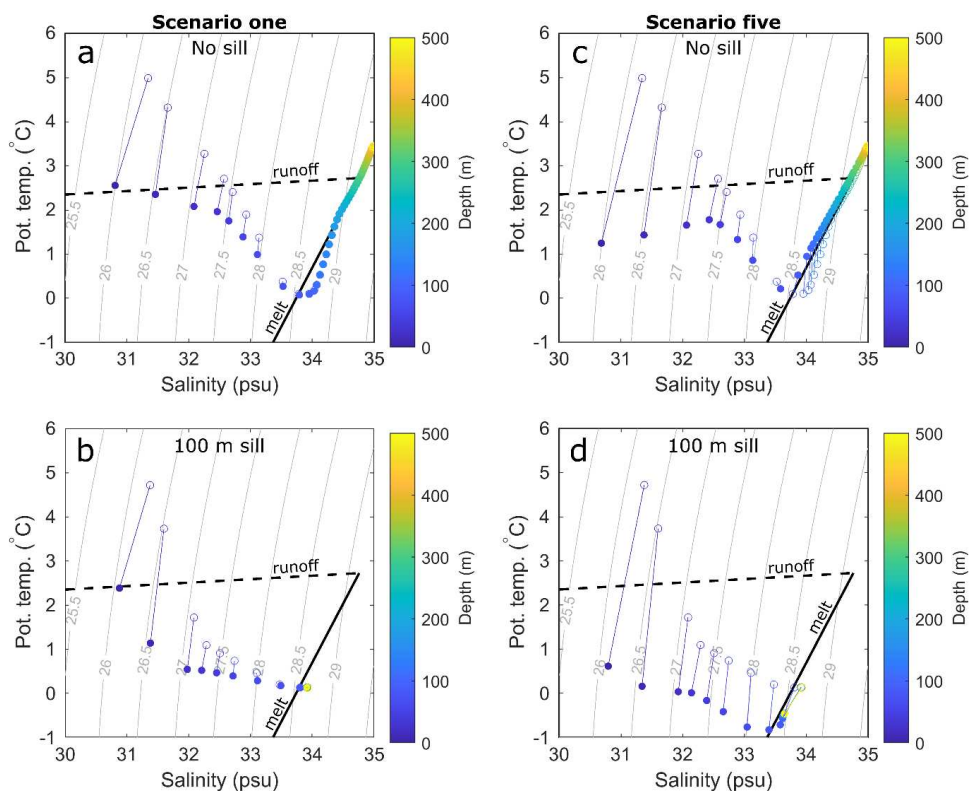


Figure 5. Glacier-adjacent temperature and salinity with (solid circles) and without icebergs (open circles) for various iceberg and sill scenarios and with *BCstandard* boundary conditions. Panels (a) and (b) show iceberg scenario one without a 100 m sill (a) and with a sill (b). Panels (c) and (d) show iceberg scenario five, without a sill (c) and with a 100 m sill (d). Solid lines joining open and closed circles indicate connected data points extracted from the same model depth.

255 properties arise due the combined effects of local iceberg melting and fjord circulation. Submarine
256 iceberg melting reduces the density of surrounding waters, causing upwelling until those waters
257 equilibrate at a new neutral buoyancy depth with respect to the fjord stratification. Within the
258 temperature-salinity space of Greenland's fjords, density is predominantly salinity controlled.
259 Therefore, the salinity stratification is little changed by iceberg melting, whilst the temperature changes
260 are much more pronounced. This means that the iceberg melt-induced migrations through temperature-
261 salinity space that are often steeper than predicted by the submarine melt mixing line (Gade, 1979).

262

263 3.2.2. Changing Atlantic Water temperature

264 We also examine the interactions between iceberg scenarios and changes to AW temperature (Fig. 6).
265 As in the PW scenarios, there is always marked cooling in the upper ~60 m of the water column and

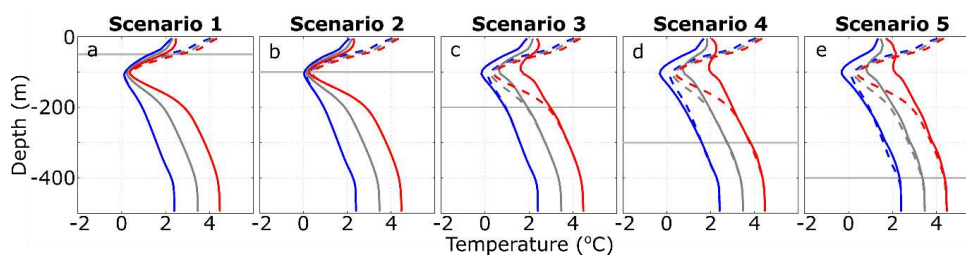


Figure 6. Steady-state glacier-adjacent water temperature for a range of initial Atlantic Water conditions and with a flat-bottomed domain. In all plots, solid and dashed lines indicate simulations with and without icebergs, respectively. Grey, blue and red lines show scenarios using the *BCstandard*, *AWcool* and *AWwarm* boundary conditions, respectively (shown in Figure 1f). The horizontal grey lines indicate the maximum iceberg keel depth in each scenario.

266 water modification below this is minimal for iceberg scenarios one and two. In iceberg scenarios three
267 to five, icebergs penetrate to a greater depth and thus into the AW layer, releasing freshwater which
268 causes upwelling of AW. In these cases, the net effect of icebergs on water properties between ~80 m
269 and the maximum iceberg keel depth depends on the balance between cooling due to localised iceberg
270 melting, and warming due to upwelling of AW. With *AWwarm*, there is a steep temperature gradient
271 between the cold PW and warmer AW layers. Consequently, upwelling of AW causes notable warming
272 in the PW layer that offsets localised iceberg-induced cooling. In the scenarios with greater iceberg
273 concentration (e.g. iceberg scenario five; Fig. 6e), the icebergs penetrate deeper into the AW layer and
274 so can induce upwelling of the deeper, warmer water, resulting in more warming and over a greater
275 depth range than in the lower iceberg concentration scenarios. However, with *AWcool*, the vertical
276 temperature gradient is reduced, so cooling due to localised iceberg melting dominates the signal
277 between the maximum iceberg draught and ~80 m.

278 This dependence of iceberg modification of glacier-adjacent water properties on the temperature
279 gradient through the AW layer is further illustrated by sensitivity tests in which the temperature of the
280 AW layer was modified in two ways relative to *BCstandard*. First, to examine whether the absolute
281 temperature of the water column affected the balance between upwelling and melting, the entire water
282 column was uniformly warmed by 1°C. With this uniform shift in temperature, the pattern of
283 temperature with depth is similar to that of *BCstandard* (compare dashed grey and red lines in Fig. 7b),
284 illustrating that the additional upwelling-driven warming with *AWwarm* is due to the steeper
285 temperature gradient between the PW and AW layers, rather than the absolute temperature of the AW.
286 Secondly, to illustrate the importance of the temperature gradient within the AW layer, we made the
287 AW layer uniformly 3.5°C. With this set of boundary conditions, upwelling-driven warming dominates
288 in the PW layer, because of upwelling of warm AW, whilst melt-driven cooling dominates in the AW
289 layer because upwelling-driven warming is muted (Fig. 7c). Thus, the average warming below ~80 m

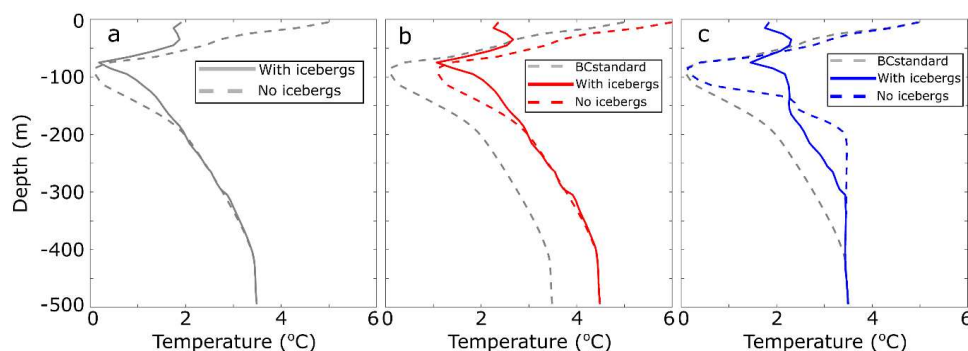


Figure 7. AW temperature gradient sensitivity tests. Panels show simulations using (a) *BCstandard*, (b) temperature profile shifted by 1°C throughout the water column, and (c) uniform initial AW temperature of 3.5°C. Steady-state conditions without icebergs using *BCstandard* (grey line) are also shown in (b) and (c) for reference.

290 that we simulate with *AWwarm* is strongly sensitive to the vertical temperature gradient, and not only
291 the average or maximum temperature of the AW.

292 With the addition of a 100 m sill, AW does not propagate into the fjord under the conditions simulated
293 here. Thus in steady-state, glacier-adjacent water properties are unaffected by AW and adopt the
294 properties of the PW layer (modified by iceberg melting and runoff). The resulting profiles therefore
295 resemble the dashed pale blue lines in Fig. 4f-j and are not shown here.

296

297 4. Discussion

298 4.1. Comparison with observations and applicability to real fjords

299 Our simulations suggest that several changes to glacier-adjacent water properties can occur due to
300 submarine iceberg melting. In almost all simulations, we simulate pronounced (>2°C) cooling in the
301 upper several tens of metres of the water column. Deeper in the water column (between ~80 m and the
302 maximum iceberg keel depth), both iceberg-induced cooling and warming can occur (e.g. Fig. 4 and 6),
303 depending on the balance between cooling due local iceberg melting and warming due to melt-driven
304 upwelling. The balance between these processes depends on the iceberg contact area at depth available
305 for local melting (and therefore cooling) and on the temperature of the upwelling water. When vertical
306 temperature gradients are steep (e.g. with *AWwarm*; Fig. 6), icebergs can cause warming between their
307 maximum keel depth and the surface layer. This is particularly apparent in the PW layer, where the
308 temperature difference between an upwelled parcel of water and that at the parcel's new neutral
309 buoyancy depth in the PW layer is greatest, and where iceberg melt rates (and therefore melt-driven
310 cooling) are generally smaller because of the low water temperatures. In contrast, when vertical



311 temperature gradients are shallower (e.g. with *AWcool*), cooling due to localised melting dominates
312 (blue lines in Fig. 7d,e and 7c). These effects tend to reduce vertical temperature variations of glacier-
313 adjacent waters compared both to simulations without icebergs and compared to conditions at the fjord
314 mouth.

315 Detailed near-glacier hydrographic observations against which to make comparisons are sparse, but
316 those that do exist provide some useful insight into the applicability of our model results to Greenland's
317 fjords. The pronounced surface and near-surface cooling (relative to conditions at the mouth) that we
318 simulate is a common feature in Greenland's fjords. For example, a transect of conductivity,
319 temperature, depth (CTD) casts along Sermilik Fjord revealed cooling of approximately 4°C in the
320 upper ~50 m (Straneo et al., 2011, 2012), which was also reproduced in a detailed modelling study of
321 Sermilik Fjord that included icebergs (Davison et al., 2020). Similar along-fjord near-surface cooling
322 has also been observed in other iceberg-congested fjords, such as Illulissat Isfjord (Beaird et al., 2017;
323 Gladish et al., 2015) and Upernavik Isfjord (Fenty et al., 2016), both in west Greenland. In Illulissat
324 Isfjord, the cold surface layer usually extends along-fjord to a shallow sill at the fjord mouth, where
325 icebergs frequently become grounded (Gladish et al., 2015).

326 Iceberg-induced changes to water properties below ~80 m are harder to identify in hydrographic
327 observations, most likely because they also contain the signature of glacial-plumes resulting from
328 subglacial discharge, or other external forcings. Our modelling suggests that, if vertical temperature
329 gradients are shallow, then icebergs can cause cooling over large depth ranges (e.g. Fig. 7c). As one
330 example, hydrographic observations in Kangerdlugssuaq Fjord showed relatively uniform near-glacier
331 temperatures with substantial cooling in both the upper 100 m and between 300 and 400 m depth,
332 relative to a transect acquired at the fjord mouth (Straneo et al., 2012), consistent with the modelling
333 results presented here. Iceberg-melt-induced warming of parts of the water column is harder to identify
334 in hydrographic observations because of the difficulty in distinguishing it from relatively warm
335 subglacial runoff-driven plume outflow.

336 To further compare our modelling results to observations, we examined CTD casts acquired as part of
337 the Oceans Melting Greenland (OMG) project (<https://omg.jpl.nasa.gov/>; data available at:
338 <https://omg.jpl.nasa.gov/portal/browse/OMGEV-AXCTD/>). As with the previous comparisons, and in
339 keeping with our simulation design, we selected pairs of CTD casts acquired less than a week apart,
340 one near or outside the fjord mouth and the other as close as possible to the tidewater glacier at the head
341 of the fjord. These profiles (Fig. 8) show many of the characteristics that we have simulated here.
342 Specifically, the profiles show that near-surface water temperatures are substantially colder adjacent to
343 tidewater glaciers compared to those observed outside each fjord, and the observed temperature
344 differences are comparable to those simulated here. In all but two (Illulissat Isfjord and Timmiarmiut
345 Fjord) of the surveyed fjords, the profiles also show warming at intermediate depths (~50-200 m)

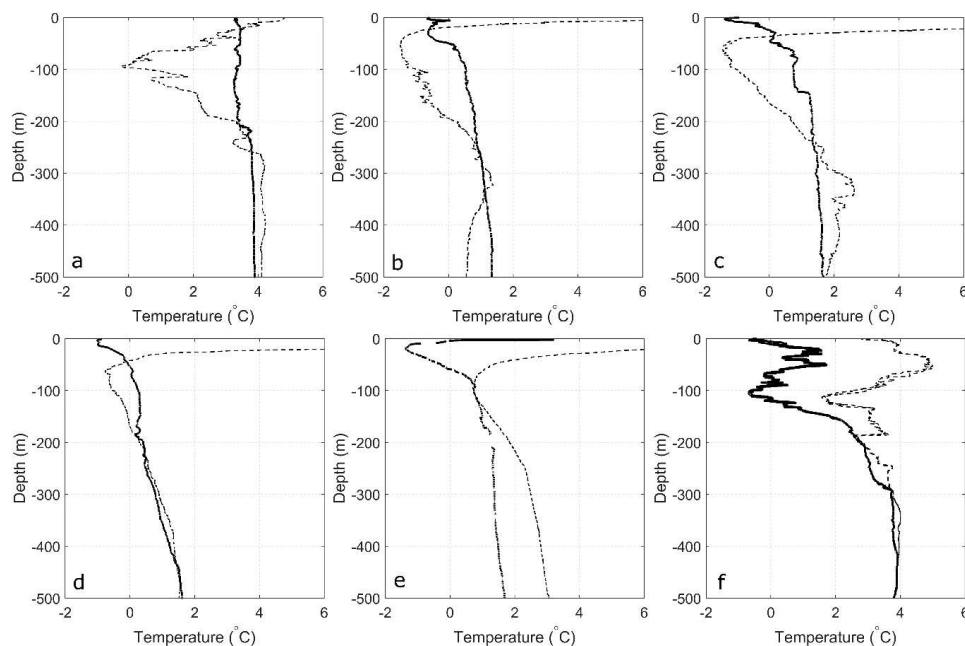


Figure 8. Fjord temperature profiles from the Oceans Melting Greenland project (<https://omg.jpl.nasa.gov/>). In panels, solid lines are profiles acquired within the fjord, close to tidewater glacier termini, and the dashed lines are acquired at or beyond the fjord mouth. Fjords (or nearest glacier) shown are (a) Sermilik Fjord, (b) Daugaard-Jensen, (c) Upernavik Isstrom, (d) Nunatakassap Sermia Fjord, (e) Ilulissat Isfjord, and (f) Timmiarmiut Fjord. Note, in (f), both an up- and down-cast are shown for the outer part of the fjord. Data are available from: <https://omg.jpl.nasa.gov/portal/browse/OMGEV-AXCTD/>

346 relative to the waters outside the fjord. These observations do not allow us to quantify the relative
347 contributions to intermediate depth warming between plume outflow and iceberg melt-induced
348 upwelling. However, we note that the vertical pattern and magnitudes of intermediate depth warming
349 are similar to those simulated here. In addition, the intermediate depth warming occurs over a large
350 depth range, which is not easily explained by plume outflow and is consistent with our simulations.
351 Some of the profiles also show notable cooling at depth (e.g. Illulissat Isfjord), which we are only able
352 to reproduce in simulations including a shallow sill. Our simulations may underestimate cooling at
353 depth because power law size-frequency distributions underestimate the number of very large icebergs
354 (Sulak et al., 2017) and because the parameter values used in our melt calculation may underestimate
355 submarine melt rates (Jackson et al., 2020).

356

357 4.2. Implications for glacier-ocean interaction

358 If iceberg-induced changes to glacier-adjacent water properties significantly affect the magnitude
359 and/or the vertical pattern of glacier submarine melting, then icebergs may play an important role in

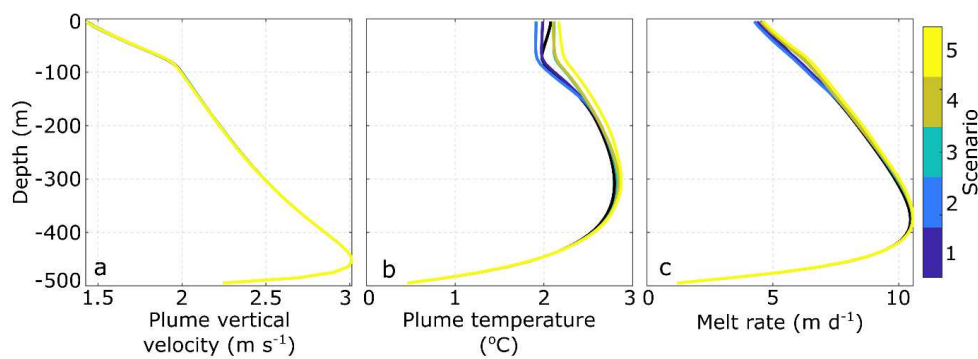


Figure 9. Plume dynamics for iceberg scenarios one to five. (a) Plume vertical velocity. (b) Plume temperature. (c) Glacier submarine melt rate in the plume. All simulations are based on *BCstandard* boundary conditions and 500 m s^{-1} runoff.

360 modifying glacier response to ocean forcing. To assess the effect of icebergs on glacier submarine
361 melting, we first consider how iceberg-melt impacts subglacial runoff-driven plume dynamics and then
362 assess how the simulated temperature changes could affect melt rates across the parts of glacier fronts
363 that are not directly affected by runoff-driven plumes.

364 To examine the effect of icebergs on subglacial discharge plume-driven glacier submarine melting, we
365 evaluate plume properties for a single set of ocean boundary conditions (*BCstandard*; Fig. 1b-d) using
366 each of the five iceberg scenarios. We find that submarine iceberg melting has negligible influence on
367 plume vertical velocity and only modest influence on plume temperature, meaning plume-induced
368 glacier submarine melt rates appear relatively insensitive to the changes in temperature and salinity
369 induced by changes in iceberg geometry, concentration and size-frequency distribution (Fig. 9).

370 Although runoff-driven plume dynamics appear to be relatively insensitive to iceberg-induced
371 modification of glacier-adjacent water properties, submarine melting distal to glacial plumes
372 ('background melting' (e.g. Slater et al., 2018)) may be more directly affected. Qualitatively, the
373 iceberg-melt-induced changes to glacier-adjacent water properties presented above suggest that iceberg
374 melt will affect background glacier melt rates in three key ways: (1) at and near the fjord surface, cooling
375 will reduce background melt rates; (2) in the PW layer, background melting will usually increase due
376 to upwelling of warmer AW, and; (3) in the AW layer, iceberg melt-induced changes in background
377 melt rates are expected to be modest, with slight increases in fjords with steep vertical temperature
378 gradients, and slight decreases in other fjords (assuming icebergs penetrate into the AW layer). These
379 effects will be more pronounced in fjords with higher concentrations of larger (and thus deeper keeled)
380 icebergs. In some fjords, then, where icebergs cause cooling near the surface and warming at depth, we
381 expect icebergs will increase glacier undercutting through impacting submarine melt rates, which may



382 in turn influence the rate and mechanism of calving (Benn et al., 2017; James et al., 2014; O’Leary and
383 Christoffersen, 2013).

384 To explore these effects quantitatively, we calculate the percentage change in background melt rate of
385 the glacier terminus due to iceberg-induced modification of glacier-adjacent water temperature (relative
386 to simulations without icebergs). Modelling studies indicate that background melt rates scale linearly
387 with ocean temperature (Sciascia et al., 2013; Slater et al., 2016; Xu et al., 2013); thus, changes in
388 temperature, T , should cause proportional changes in background melting (Jackson et al., 2014). We
389 choose to focus on relative changes in melt rate, rather than absolute changes, because of poor
390 constraints on important melt rate parameter values (Jackson et al., 2020). We calculate the relative
391 change in submarine melt rate, SMR , following Jackson et al. (2014), as:

$$392 \quad \Delta SMR = \frac{(T_{ib} - T_f) - (T_{nib} - T_f)}{(T_{nib} - T_f)} 100$$

393 where the subscripts ib and nib indicate simulations with ‘icebergs’ and ‘no icebergs’, respectively, and
394 T_f is the *in-situ* freezing point, given by:

$$395 \quad T_f = \lambda_1 S + \lambda_2 + \lambda_3 z$$

396 where λ_{1-3} are constants representing the freezing point slope ($-0.0573 \text{ }^\circ\text{C psu}^{-1}$), offset (0.0832°C) and
397 depth ($0.000761^\circ\text{C m}^{-1}$), respectively. S is the local salinity (horizontally averaged within 2 km of the
398 terminus) and z is depth in the water column.

399 Using this approach, we find that the impact on water properties resulting from iceberg melt
400 substantially modifies background glacier submarine melt rates. Firstly, in the upper 50 m and using
401 *BCstandard*, iceberg melt causes a 34.9% reduction in melt rate on average. Even in iceberg scenario
402 one, iceberg melt causes a 29.5% reduction in melt rate over this depth range. Secondly, between 100
403 and 200 m depth, iceberg melt causes a 13.5% increase in melt rate on average when using *BCstandard*,
404 but this increases to 59.2% when using *PWcool* (for which warming of the PW layer due to upwelling
405 is most pronounced). Changes in iceberg melt rates in the AW layer are minimal, with the most
406 pronounced effect being a 5.4% increase in the 200-400 m depth range using iceberg scenario five and
407 *PWwarm*. When averaged through the entire water column, these effects largely compensate for each
408 other, resulting in a net 3.1% decrease in melt rates with *BCstandard*. Overall therefore, this analysis
409 suggests that iceberg melt can influence the vertical pattern of glacier terminus background melting by
410 decreasing melt rates at the surface and increasing them in the PW layer, with minimal changes in the
411 AW layer.

412 As well as affecting glacier-adjacent water temperatures, iceberg melt likely affects submarine melt
413 rates in other ways not examined here. For example, the cooling and freshening of the surface and near-
414 surface layers induced by iceberg melting may prevent or hinder plume surfacing (De Andrés et al.,



415 2020), and may expedite sea ice formation after the melt season, promoting the development of an ice
416 mélange. In addition, mechanical iceberg breakup, iceberg calving and iceberg rotation can cause
417 vigorous mixing of fjord waters which can temporarily increase glacier and iceberg submarine melt
418 rates (Enderlin et al., 2018), and increases the iceberg-ocean contact area available for melting. Iceberg-
419 melt-induced invigoration of fjord circulation can increase oceanic heat flux towards tidewater glaciers
420 (Davison et al., 2020), likely resulting in faster terminus submarine melting. Icebergs likely also exert
421 a mechanical influence on the circulation and plume dynamics at the ice-ocean interface (Amundson et
422 al., 2020), and may prevent plume surfacing (Xie et al., 2019).

423

424 **4.3. Implications for oceanic forcing of ice sheet-scale models**

425 Current state-of-the-art projections of dynamic mass loss from the Greenland Ice Sheet (Goelzer et al.,
426 2020) are forced by far-field ocean temperature profiles, provided by ocean modelling output that does
427 not include fjord-scale processes (except for the obstruction of shelf-water intrusion by shallow sills)
428 (Slater et al., 2019, 2020). The results presented here suggest that such an approach is broadly
429 appropriate for fjords with maximum iceberg keel depths of less than 200 m and iceberg concentrations
430 less than ~20% on average, where iceberg modification of glacier-adjacent water properties appears to
431 be limited other than in the upper several tens of metres (Figs 4 and 6). The majority of Greenland's
432 fjords likely fall into this category (Mankoff et al., 2019; Sulak et al., 2017). Even in such fjords,
433 however, this approach would not capture the surface and near-surface cooling caused by iceberg
434 melting. In order to capture this near surface cooling, one relatively simple modification to such an
435 approach could be to reduce surface water temperature to close to the *in-situ* melting point during winter
436 periods, and proportionally to the iceberg surface area at the fjord surface during summer periods.

437 However, in fjords hosting icebergs with keel depth greater than or equal to 200 m and with average
438 concentrations of more than ~20% (i.e. our iceberg scenario three or higher), iceberg modification of
439 glacier-adjacent water properties becomes increasingly important. In such fjords that also exhibit
440 relatively shallow sills, icebergs act to cool glacier-adjacent water throughout the water column, with
441 the amount of cooling proportional to the draught and concentration of the icebergs, as well as to the
442 temperature of the ambient water at the fjord mouth (Fig. 4). In such fjords that do not have shallow
443 sills, the effect is more complicated, with both iceberg-melt-induced warming and cooling, depending
444 on the vertical temperature gradient of the water column and iceberg concentration at depth. Overall,
445 these changes to the water column temperature can cause non-negligible (up to several tens of percent)
446 changes in terminus submarine melt rates across the large areas of the calving front that are not directly
447 affected by plume-inducing subglacial discharge. The vertical pattern of changes to terminus submarine
448 melt rates (reduced near the surface and increased at intermediate depths) induced by iceberg melting
449 is expected to exacerbate undercutting of glacier termini, with potentially important impacts on calving



450 rates (Benn et al., 2017; Ma and Bassis, 2019; O’Leary and Christoffersen, 2013; Todd and
451 Christoffersen, 2014). Although fjords hosting icebergs this large and numerous are relatively few in
452 number, it is these fjords (and the glaciers hosted by them) that contribute the most to dynamic mass
453 loss from the Greenland Ice Sheet (Enderlin et al., 2014; Khan et al., 2020).

454

455 **4.4. Transience vs steady-state**

456 All of the results presented here were extracted from the final ten days of simulations that were run to
457 a quasi-steady state (i.e. the variable of interest had stabilised). In our domains without sills, steady-
458 state of temperature and salinity was generally reached after just ten to thirty days. However, our
459 simulations with sills could take as many as one thousand days to reach such a steady state because
460 fjord-shelf exchange is reduced. For an equivalent steady-state to be reached in reality, open ocean
461 conditions, runoff and iceberg size and distribution would also have to remain quasi-stable for an
462 equivalent time period. In reality, this is unlikely to occur (particularly in fjords with shallow sills)
463 because runoff and coastal and open ocean conditions change on sub-seasonal to seasonal timescales
464 (Moon et al., 2017; Mortensen et al., 2014; Noël et al., 2016; Sutherland et al., 2014; Sutherland and
465 Pickart, 2008). In reality therefore, glacier-adjacent water properties in fjords with shallow sills are
466 likely a complex amalgamation of temporally-evolving source waters, modified by processes operating
467 within the fjord. In addition, some variations in coastal conditions can be transmitted towards glaciers
468 very rapidly. During winter, strong wind events on the east coast of Greenland drive fast shelf-forced
469 flows (or intermediary currents) in glacial fjords, delivering coastal waters to tidewater glaciers over
470 just a period of a few days, and potentially reducing the magnitude of iceberg-driven modification
471 (Jackson et al., 2014, 2018). Such currents are strongest in winter, when hydrographic observations are
472 sparse, so this remains speculative.

473

474 **5. Conclusions**

475 We have used a general circulation model (MITgcm) to quantify the effect of submarine iceberg melting
476 on glacier-adjacent water properties in an idealised fjord domain. A large range of iceberg
477 concentrations, keel depths and size-frequency distributions were examined to represent the range of
478 iceberg conditions found in Greenland’s marine terminating glacier fjords. We focused primarily on
479 iceberg-melt-induced changes to glacier-adjacent water temperatures throughout the water column,
480 because of their principal importance to glacier-submarine melting.

481 Our results suggest that icebergs can substantially modify glacier-adjacent water properties and that the
482 precise impact depends on iceberg size and on the temperature profile and stratification of water within
483 and beyond the fjord. In particular, we find that (1) temperature in the upper ~60 m of the water column
484 is reduced by several degrees Celsius over a wide range of iceberg scenarios; (2) fjords with more and



485 deeper icebergs are subject to greater iceberg-melt-induced modification, which can result in either
486 cooling or warming at different depths depending on the balance between melt-driven cooling and
487 upwelling-driven warming, which in turn depends on fjord temperature stratification, and; (3) when
488 icebergs extend to or below the fjord mouth sill depth, they can cause significant cooling throughout
489 the water column. Particularly with regard to point (2), our results highlight that oceanic forcing of large
490 fast-flowing glaciers, which contribute the most to ice sheet dynamic mass loss, in existing projections
491 of tidewater glacier dynamics is strongly affected by ignoring the impact of icebergs on fjord water
492 properties. The iceberg-induced changes to the vertical temperature profile of glacier-adjacent waters
493 identified here are likely to reduce submarine melt rates at and near the fjord surface while increasing
494 them in the PW layer, which may influence the rate and mechanism of calving by exacerbating glacier
495 terminus undercutting. Our results therefore identify a critical need to develop simple parameterisations
496 of iceberg-induced modification of fjord waters, and other fjord-scale processes, to better constrain
497 oceanic forcing of tidewater glaciers.

498

499

500 **Code availability**

501 MITgcm is freely available at http://mitgcm.org/public/source_code.html. The IcePlume module is
502 available from Tom Cowton on request. The IceBerg module is available at
503 <https://zenodo.org/record/3979647#.YWAayNrMKUk> or from Benjamin Davison on request.

504

505 **Data availability**

506 Data required to reproduce the analysis and figures in this manuscript will be made available upon
507 publication.

508

509 **Author contributions**

510 BD and TC conceived the study. BD developed the model code with support from TC and AS. BD
511 designed and conducted the simulations and analysis, and led the manuscript write up. TC, FC, AS and
512 PN supported the interpretation of the model results and contributed to the preparation of the
513 manuscript.

514

515 **Competing interests**



516 The authors declare that they have no conflict of interest.

517

518 **Acknowledgements**

519 BD was funded by a PhD studentship provided by the Scottish Alliance for Geosciences, Environment
520 and Society (SAGES) and the University of St Andrews, UK. The simulations were conducted on the
521 Sheffield Advanced Research Computer (ShARC).

522 **References**

523 Amundson, J. M., Kienholz, C., Hager, A. O., Jackson, R. H., Motyka, R. J., Nash, J. D. and
524 Sutherland, D. A.: Formation, flow and break-up of ephemeral ice mélange at LeConte Glacier and
525 Bay, Alaska, *J. Glaciol.*, 66(258), 577–590, doi:10.1017/jog.2020.29, 2020.

526 De Andrés, E., Slater, D. A., Straneo, F., Otero, J., Das, S. and Navarro, F.: Surface emergence of
527 glacial plumes determined by fjord stratification, *Cryosph. Discuss.*, in review(January),
528 doi:https://doi.org/10.5194/tc-2019-264, 2020.

529 Barker, A., Sayed, M. and Carrieres, T.: Determination of iceberg draft, mass and cross-sectional
530 areas, *Proc. 14th Int. Offshore Polar Eng. Conf.*, 899–904, 2004.

531 Beaird, N., Straneo, F. and Jenkins, W.: Characteristics of meltwater export from Jakobshavn Isbræ
532 and Ilulissat Icefjord, *Ann. Glaciol.*, 58(74), 107–117, doi:10.1017/aog.2017.19, 2017.

533 Beaird, N. L., Straneo, F. and Jenkins, W.: Export of Strongly Diluted Greenland Meltwater From a
534 Major Glacial Fjord, *Geophys. Res. Lett.*, 45(9), 4163–4170, doi:10.1029/2018GL077000, 2018.

535 Benn, D. I., Aström, J., Zwinger, T., Todd, J., Nick, F. M., Cook, S., Hulton, N. R. J. and Luckman,
536 A.: Melt-under-cutting and buoyancy-driven calving from tidewater glaciers: New insights from
537 discrete element and continuum model simulations, *J. Glaciol.*, 63(240), 691–702,
538 doi:10.1017/jog.2017.41, 2017.

539 Carroll, D., Sutherland, D. A., Hudson, B., Moon, T., Catania, G. A., Shroyer, E. L., Nash, J. D.,
540 Bartholomäus, T. C., Felikson, D., Stearns, L. A., Noël, Y. and Van Den Broeke, M. R.: The impact
541 of glacier geometry on meltwater plume structure and submarine melt in Greenland fjords, *Geophys.*
542 *Res. Lett.*, 43, doi:10.1002/2016GL070170, 2016.

543 Cowton, T., Slater, D., Sole, A., D. G. and Niewnow, P.: Modeling the impact of glacial runoff on
544 fjord circulation and submarine melt rate using a new subgrid-scale parameterization for glacial
545 plumes, *J. Geophys. Res. Ocean.*, 120, 1–17, doi:10.1002/2014JC010324, 2015.

546 Cowton, T., Sole, A., Nienow, P., Slater, D., Wilton, D. and Hanna, E.: Controls on the transport of



- 547 oceanic heat to Kangerdlugssuaq Glacier, East Greenland, *J. Glaciol.*, 1–14,
548 doi:10.1017/jog.2016.117, 2016.
- 549 Davison, B. J., Cowton, T. R., Cottier, F. R. and Sole, A. J.: Iceberg melting substantially modifies
550 oceanic heat flux towards a major Greenlandic tidewater glacier, *Nat. Commun.*, 11(1), 1–13,
551 doi:10.1038/s41467-020-19805-7, 2020.
- 552 Dowdeswell, J. A., Whittington, R. J. and Hodgkins, R.: The sizes, frequencies, and freeboards of
553 East Greenland icebergs observed using ship radar and sextant, *J. Geophys. Res.*, 97(C3), 3515,
554 doi:10.1029/91JC02821, 1992.
- 555 Edwards, T. L., Nowicki, S., Marzeion, B., Hock, R., Goelzer, H., Seroussi, H., Jourdain, N. C.,
556 Slater, D. A., Turner, F. E., Smith, C. J., McKenna, C. M., Simon, E., Abe-Ouchi, A., Gregory, J. M.,
557 Larour, E., Lipscomb, W. H., Payne, A. J., Shepherd, A., Agosta, C., Alexander, P., Albrecht, T.,
558 Anderson, B., Asay-Davis, X., Aschwanden, A., Barthel, A., Bliss, A., Calov, R., Chambers, C.,
559 Champollion, N., Choi, Y., Cullather, R., Cuzzone, J., Dumas, C., Felikson, D., Fettweis, X., Fujita,
560 K., Galton-Fenzi, B. K., Gladstone, R., Golledge, N. R., Greve, R., Hattermann, T., Hoffman, M. J.,
561 Humbert, A., Huss, M., Huybrechts, P., Immerzeel, W., Kleiner, T., Kraaijenbrink, P., Le clec'h, S.,
562 Lee, V., Leguy, G. R., Little, C. M., Lowry, D. P., Malles, J. H., Martin, D. F., Maussion, F.,
563 Morlighem, M., O'Neill, J. F., Nias, I., Pattyn, F., Pelle, T., Price, S. F., Quiquet, A., Radić, V.,
564 Reese, R., Rounce, D. R., Rückamp, M., Sakai, A., Shafer, C., Schlegel, N. J., Shannon, S., Smith, R.
565 S., Straneo, F., Sun, S., Tarasov, L., Trusel, L. D., Van Breedam, J., van de Wal, R., van den Broeke,
566 M., Winkelmann, R., Zekollari, H., Zhao, C., Zhang, T. and Zwinger, T.: Projected land ice
567 contributions to twenty-first-century sea level rise, *Nature*, 593(7857), 74–82, doi:10.1038/s41586-
568 021-03302-y, 2021.
- 569 Enderlin, E. M., Howat, I. M., Jeong, S., Noh, M. J., van Angelen, J. H. and Van den Broeke, M. R.:
570 An improved mass budget for the Greenland ice sheet, *Geophys. Res. Lett.*, 41, 866–872,
571 doi:10.1002/2013GL059010., 2014.
- 572 Enderlin, E. M., Hamilton, G. S., Straneo, F. and Sutherland, D. A.: Iceberg meltwater fluxes
573 dominate the freshwater budget in Greenland's iceberg-congested glacial fjords, *Geophys. Res. Lett.*,
574 43(21), 11,287–11,294, doi:10.1002/2016GL070718, 2016.
- 575 Enderlin, E. M., Carrigan, C. J., Kochtitzky, W. H., Cuadros, A., Moon, T. and Hamilton, G. S.:
576 Greenland Iceberg Melt Variability from High-Resolution Satellite Observations, *Cryosph.*,
577 (September), 1–17, 2018.
- 578 Fenty, I., Willis, J., Khazendar, A., Dinardo, S., Forsberg, R., Fukumori, I., Holland, D., Jakobsson,
579 M., Moller, D., Morison, J., Münchow, A., Rignot, E., Schodlok, M., Thompson, A., Tinto, K.,
580 Rutherford, M. and Trenholm, N.: Oceans Melting Greenland: Early Results from NASA's Ocean-Ice



- 581 Mission in Greenland, *Oceanography*, 29(4), 72–83, doi:10.5670/oceanog.2016.100, 2016.
- 582 Fraser, N. J. and Inall, M. E.: Influence of Barrier Wind Forcing on Heat Delivery Toward the
583 Greenland Ice Sheet, *J. Geophys. Res. Ocean.*, 123(4), 2513–2538, doi:10.1002/2017JC013464, 2018.
- 584 Gladish, C. V., Holland, D. M., Rosing-Asvid, A., Behrens, J. W. and Boje, J.: Oceanic Boundary
585 Conditions for Jakobshavn Glacier: Part I. Variability and Renewal of Ilulissat Icefjord Waters, 2001-
586 2014, *J. Phys. Oceanogr.*, 45, doi:10.1175/JPO-D-14-0044.1, 2015.
- 587 Goelzer, H., Nowicki, S., Payne, A., Larour, E., Seroussi, H., Lipscomb, W. H., Gregory, J., Abe-
588 Ouchi, A., Shepherd, A., Simon, E., Agosta, C., Alexander, P., Aschwanden, A., Barthel, A., Calov,
589 R., Chambers, C., Choi, Y., Cuzzone, J., Dumas, C., Edwards, T., Felikson, D., Fettweis, X.,
590 Golledge, N. R., Greve, R., Humbert, A., Huybrechts, P., Le Clec'H, S., Lee, V., Leguy, G., Little, C.,
591 Lowry, D., Morlighem, M., Nias, I., Quiquet, A., Rückamp, M., Schlegel, N. J., Slater, D. A., Smith,
592 R., Straneo, F., Tarasov, L., Van De Wal, R. and Van Den Broeke, M.: The future sea-level
593 contribution of the Greenland ice sheet: A multi-model ensemble study of ISMIP6, *Cryosphere*, 14(9),
594 3071–3096, doi:10.5194/tc-14-3071-2020, 2020.
- 595 Holland, D. M. and Jenkins, A.: Modeling Thermodynamic Ice–Ocean Interactions at the Base of an
596 Ice Shelf, *J. Phys. Oceanogr.*, 29(8), 1787–1800, doi:10.1175/1520-
597 0485(1999)029<1787:MTIOIA>2.0.CO;2, 1999.
- 598 Inall, M. E., Murray, T., Cottier, F. R., Scharrer, K. and Boyd, T. J.: Oceanic heat delivery via
599 Kangerdlugssuaq Fjord to the south-east Greenland ice sheet, *J. Geophys. Res. Ocean.*, 631–645,
600 doi:10.1002/2013JC009295. Received, 2014.
- 601 Jackson, R. H. and Straneo, F.: Heat, salt, and freshwater budgets for a glacial fjord in Greenland, *J.*
602 *Phys. Oceanogr.*, 0(0), 2735–2768, doi:10.1175/JPO-D-15-0134.1, 2016.
- 603 Jackson, R. H., Straneo, F. and Sutherland, D. a.: Externally forced fluctuations in ocean temperature
604 at Greenland glaciers in non-summer months, *Nat. Geosci.*, 7(June), 1–6, doi:10.1038/ngeo2186,
605 2014.
- 606 Jackson, R. H., Shroyer, E. L., Nash, J. D., Sutherland, D. A., Carroll, D., Fried, M. J., Catania, G. A.,
607 Bartholomaeus, T. C. and Stearns, L. A.: Near-glacier surveying of a subglacial discharge plume:
608 Implications for plume parameterizations, *Geophys. Res. Lett.*, 44(13), 6886–6894,
609 doi:10.1002/2017GL073602, 2017.
- 610 Jackson, R. H., Lentz, S. J. and Straneo, F.: The dynamics of shelf forcing in Greenlandic fjords, *J.*
611 *Phys. Oceanogr.*, 48(11), 2799–2827, doi:10.1175/JPO-D-18-0057.1, 2018.
- 612 Jackson, R. H., Nash, J. D., Kienholz, C., Sutherland, D. A., Amundson, J. M., Motyka, R. J.,



- 613 Winters, D., Skillingstad, E. and Pettit, E. C.: Meltwater Intrusions Reveal Mechanisms for Rapid
614 Submarine Melt at a Tidewater Glacier, *Geophys. Res. Lett.*, 47(2), doi:10.1029/2019GL085335,
615 2020.
- 616 Jakobsson, M., Mayer, L. A., Nilsson, J., Stranne, C., Calder, B., O'Regan, M., Farrell, J. W., Cronin,
617 T. M., Brüchert, V., Chawarski, J., Eriksson, B., Fredriksson, J., Gemery, L., Glueder, A., Holmes, F.
618 A., Jerram, K., Kirchner, N., Mix, A., Muchowski, J., Prakash, A., Reilly, B., Thornton, B., Ulfsbo,
619 A., Weidner, E., Åkesson, H., Handl, T., Ståhl, E., Boze, L.-G., Reed, S., West, G. and Padman, J.:
620 Ryder Glacier in northwest Greenland is shielded from warm Atlantic water by a bathymetric sill,
621 *Commun. Earth Environ.*, 1(1), 1–10, doi:10.1038/s43247-020-00043-0, 2020.
- 622 James, T. D., Murray, T., Selmes, N., Scharrer, K. and O'Leary, M.: Buoyant flexure and basal
623 crevassing in dynamic mass loss at Helheim Glacier, *Nat. Geosci.*, 7(8), 593–596,
624 doi:10.1038/ngeo2204, 2014.
- 625 Jenkins, A.: Convection-Driven Melting near the Grounding Lines of Ice Shelves and Tidewater
626 Glaciers, *J. Phys. Oceanogr.*, 41(12), 2279–2294, doi:10.1175/JPO-D-11-03.1, 2011.
- 627 Khan, S. A., Bjørk, A. A., Bamber, J. L., Morlighem, M., Bevis, M., Kjær, K. H., Mouginot, J.,
628 Løkkegaard, A., Holland, D. M., Aschwanden, A., Zhang, B., Helm, V., Korsgaard, N. J., Colgan, W.,
629 Larsen, N. K., Liu, L., Hansen, K., Barletta, V., Dahl-Jensen, T. S., Søndergaard, A. S., Csatho, B.,
630 M., Sasgen, I., Box, J. and Schenk, T.: Centennial response of Greenland's three largest outlet
631 glaciers, *Nat. Commun.*, 11(1), 1–9, doi:10.1038/s41467-020-19580-5, 2020.
- 632 Kimura, S., Holland, P. R., Jenkins, A. and Piggott, M.: The effect of meltwater plumes on the
633 melting of a vertical glacier face, *J. Phys. Oceanogr.*, 44(12), 3099–3117, doi:10.1175/JPO-D-13-
634 0219.1, 2014.
- 635 Luthi, M., Funk, M., Iken, A., Gogineni, S. and Truffer, M.: Mechanisms of fast flow in Jakobshavn
636 Isbræ, Greenland, Part III: measurements of ice deformation, temperature and cross-
637 borehole conductivity in boreholes to the bedrock, *J. Glaciol.*, 48(162), 369–385,
638 doi:10.3189/172756502781831322, 2002.
- 639 Ma, Y. and Bassis, J. N.: The Effect of Submarine Melting on Calving From Marine Terminating
640 Glaciers, *J. Geophys. Res. Earth Surf.*, 124(2), 334–346, doi:10.1029/2018JF004820, 2019.
- 641 Mankoff, K. D., Solgaard, A., Colgan, W., Ahlstrøm, A. P., Abbas Khan, S. and Fausto, R. S.:
642 Greenland Ice Sheet solid ice discharge from 1986 through March 2020, *Earth Syst. Sci. Data*, 12(2),
643 1367–1383, doi:10.5194/essd-12-1367-2020, 2019.
- 644 Mankoff, K. D., Noël, B., Fettweis, X., Ahlstrøm, A. P., Colgan, W., Kondo, K., Langley, K.,
645 Sugiyama, S., Van As, D. and Fausto, R. S.: Greenland liquid water discharge from 1958 through



- 646 2019, *Earth Syst. Sci. Data*, 12(4), 2811–2841, doi:10.5194/essd-12-2811-2020, 2020.
- 647 Marshall, J., Adcroft, A., Hill, C., Perelman, L. and Heisey, C.: A finite-volume, incompressible
648 Navier Stokes model for studies of the ocean on parallel computers, *J. Geophys. Res.*, 102(C3), 5753,
649 doi:10.1029/96JC02775, 1997a.
- 650 Marshall, J., Hill, C., Perelman, L. and Adcroft, A.: Hydrostatic, quasi-hydrostatic, and
651 nonhydrostatic ocean modeling, *J. Geophys. Res.*, 102(C3), 5733, doi:10.1029/96JC02776, 1997b.
- 652 Meredith, M., Sommerkorn, M., Cassotta, S., Derksen, C., Ekaykin, A., Hollowed, A., Kofinas, G.,
653 Mackintosh, A., Melbourne-Thomas, J., Muelbert, M. M. C., Ottersen, G., Pritchard, H. and Schuur,
654 E. A. G.: Special Report on Ocean and Cryosphere in a Changing Climate: Polar Regions, , 203–320,
655 doi:10.1016/S1366-7017(01)00066-6, 2020.
- 656 Moon, T., Sutherland, D. A., Carroll, D., Felikson, D., Kehrl, L. and Straneo, F.: Subsurface iceberg
657 melt key to Greenland fjord freshwater budget, *Nat. Geosci.*, doi:10.1038/s41561-017-0018-z, 2017.
- 658 Mortensen, J., Bendtsen, J., Lennert, K. and Rysgaard, S.: Seasonal variability of the circulation
659 system in a west Greenland tidewater outlet glacier fjord, Godthåbsfjord (64°N), *J. Geophys. Res.*
660 *Earth Surf.*, 2591–2603, doi:10.1002/2014JF003267., 2014.
- 661 Moyer, A. N., Sutherland, D. A., Nienow, P. W. and Sole, A. J.: Seasonal Variations in Iceberg
662 Freshwater Flux in Sermilik Fjord, Southeast Greenland From Sentinel-2 Imagery, *Geophys. Res.*
663 *Let.*, 46(15), 8903–8912, doi:10.1029/2019GL082309, 2019.
- 664 Noël, B., Berg, W. J. Van De, Machguth, H., Lhermitte, S., Howat, I. and Fettweis, X.: A daily , 1 km
665 resolution dataset of downscaled Greenland ice sheet surface mass balance (1958-2015), *Cryosph.*
666 *Discuss.*, (May), 1–29, doi:10.5194/tc-2016-145, 2016.
- 667 O’Leary, M. and Christoffersen, P.: Calving on tidewater glaciers amplified by submarine frontal
668 melting, *Cryosphere*, 7, 119–128, doi:10.5194/tc-7-119-2013, 2013.
- 669 Rezvanbehbahani, S., Stearns, L. A., Keramati, R., Shankar, S. and van der Veen, C. J.: Significant
670 contribution of small icebergs to the freshwater budget in Greenland fjords, *Commun. Earth Environ.*,
671 1(1), 1–7, doi:10.1038/s43247-020-00032-3, 2020.
- 672 Sciascia, R., Straneo, F., Cenedese, C. and Heimbach, P.: Seasonal variability of submarine melt rate
673 and circulation in an East Greenland fjord, *J. Geophys. Res. Ocean.*, 118(5), 2492–2506,
674 doi:10.1002/jgrc.20142, 2013.
- 675 Slater, D. A., Nienow, P. W., Cowton, T. R., Goldberg, D. N. and Sole, A. J.: Effect of near-terminus
676 subglacial hydrology on tidewater glacier submarine melt rates, *Geophys. Res. Let.*, 1–8,
677 doi:10.1002/2014GL062494.1., 2015.



- 678 Slater, D. A., Goldberg, D. N., Nienow, P. W. and Cowton, T. R.: Scalings for Submarine Melting at
679 Tidewater Glaciers from Buoyant Plume Theory, *J. Phys. Oceanogr.*, 46, 1839–1855,
680 doi:10.1175/JPO-D-15-0132.1, 2016.
- 681 Slater, D. A., Straneo, F., Das, S. B., Richards, C. G., Wagner, T. J. W. and Nienow, P. W.: Localized
682 Plumes Drive Front-Wide Ocean Melting of A Greenlandic Tidewater Glacier, *Geophys. Res. Lett.*,
683 45(22), 12,350–12,358, doi:10.1029/2018GL080763, 2018.
- 684 Slater, D. A., Straneo, F., Felikson, D., Little, C. M., Goelzer, H., Fettweis, X. and Holte, J.:
685 Estimating Greenland tidewater glacier retreat driven by submarine melting, *Cryosphere*, 13(9),
686 2489–2509, doi:10.5194/tc-13-2489-2019, 2019.
- 687 Slater, D. A., Felikson, D., Straneo, F., Goelzer, H., Little, C. M., Morlighem, M., Fettweis, X. and
688 Nowicki, S.: Twenty-first century ocean forcing of the Greenland ice sheet for modelling of sea level
689 contribution, *Cryosphere*, 14(3), 985–1008, doi:10.5194/tc-14-985-2020, 2020.
- 690 Straneo, F. and Heimbach, P.: North Atlantic warming and the retreat of Greenland’s outlet glaciers,
691 *Nature*, 504, 36–43, doi:10.1038/nature12854, 2013.
- 692 Straneo, F., Hamilton, G. S., Sutherland, D. A., Stearns, L. A., Davidson, F., Hammill, M. O.,
693 Stenson, G. B. and Rosing-Asvid, A.: Rapid circulation of warm subtropical waters in a major glacial
694 fjord in East Greenland, *Nat. Geosci.*, 3(3), 182–186, doi:10.1038/ngeo764, 2010.
- 695 Straneo, F., Curry, R. G., Sutherland, D. a., Hamilton, G. S., Cenedese, C., Våge, K. and Stearns, L.
696 a.: Impact of fjord dynamics and glacial runoff on the circulation near Helheim Glacier, *Nat. Geosci.*,
697 4(5), 322–327, doi:10.1038/ngeo1109, 2011.
- 698 Straneo, F., Sutherland, D. a., Holland, D., Gladish, C., Hamilton, G. S., Johnson, H. L., Rignot, E.,
699 Xu, Y. and Koppes, M.: Characteristics of ocean waters reaching Greenland’s glaciers, *Ann. Glaciol.*,
700 53(60), 202–210, doi:10.3189/2012AoG60A059, 2012.
- 701 Sulak, D. J., Sutherland, D. A., Enderlin, E. M., Stearns, L. A. and Hamilton, G. S.: Iceberg properties
702 and distributions in three Greenlandic fjords using satellite imagery, *Ann. Glaciol.*, (May), 1–15,
703 doi:10.1017/aog.2017.5, 2017.
- 704 Sutherland, D., Straneo, F. and Pickart, R. S.: Characteristics and dynamics of two major greenland
705 glacial fjords, *J. Geophys. Res. Earth Surf.*, 2121–2128, doi:10.1002/jgrc.20224, 2014.
- 706 Sutherland, D. A. and Pickart, R. S.: The East Greenland Coastal Current: Structure, variability, and
707 forcing, *Prog. Oceanogr.*, 78(1), 58–77, doi:10.1016/j.pocean.2007.09.006, 2008.
- 708 Sutherland, D. A. and Straneo, F.: Estimating ocean heat transports and submarine melt rates in
709 sermilik fjord, greenland, using lowered acoustic doppler current profiler (LADCP) velocity profiles,



- 710 Ann. Glaciol., 53(60), 50–58, doi:10.3189/2012AoG60A050, 2012.
- 711 Sutherland, D. A., Jackson, R. H., Kienholz, C., Amundson, J. M., Dryer, W. P., Duncan, D., Eidam,
712 E. F., Motyka, R. J. and Nash, J. D.: Direct observations of submarine melt and subsurface geometry
713 at a tidewater glacier, Science (80-.), 365(6451), 369–374, doi:10.1126/science.aax3528, 2019.
- 714 Todd, J. and Christoffersen, P.: Are seasonal calving dynamics forced by buttressing from ice
715 mélange or undercutting by melting? Outcomes from full-Stokes simulations of Store Glacier, West
716 Greenland, Cryosph., 8(6), 2353–2365, doi:10.5194/tc-8-2353-2014, 2014.
- 717 Xie, S., Dixon, T. H., Holland, D. M., Voytenko, D. and Vaňková, I.: Rapid iceberg calving following
718 removal of tightly packed pro-glacial mélange, Nat. Commun., 10(1), doi:10.1038/s41467-019-
719 10908-4, 2019.
- 720 Xu, Y., Rignot, E., Menemenlis, D. and Koppes, M.: Numerical experiments on subaqueous melting
721 of Greenland tidewater glaciers in response to ocean warming and enhanced subglacial discharge,
722 Ann. Glaciol., 53(60), 229–234, doi:10.3189/2012AoG60A139, 2012.
- 723 Xu, Y., Rignot, E., Fenty, I., Menemenlis, D. and Flexas, M. M.: Subaqueous melting of Store
724 Glacier, west Greenland from three-dimensional, high-resolution numerical modeling and ocean
725 observations, Geophys. Res. Lett., 40, 4648–4653, doi:10.1002/grl.50825, 2013.
- 726
- 727